An-Najah University Journal for Research – A

Natural Sciences

Shot Peening for Improving Surface Integrity and Corrosion Resistance of DMLS-Fabricated Cu–Ni Alloys

Rajesh R[1], Mithun Vinayaka Kulkarni[2]*, Bincy Rose Vergis[3], P Sampathkumaran[4], S Anand Kumar[5]

Type: Full Article. Received: 14th Mar. 2025, Accepted: 19th Apr. 2026, Published: ××××, DOI: ××××

Received Accepted, In Press

Abstract: Surface defects inherent to Direct Metal Laser Sintering (DMLS) can significantly degrade the corrosion resistance of Cu–Ni alloys in chloride-containing environments. This study investigates the combined influence of DMLS processing parameters (laser scan speed and layer thickness) and shot peening (SP) post-treatment on the surface integrity and corrosion behaviour of additively manufactured Cu–Ni alloys. Porosity, surface roughness, microhardness, residual stress, and corrosion rate were characterised using optical microscopy, scanning electron microscopy (SEM), and energy-dispersive X-ray spectroscopy (EDS). The results show that increasing layer thickness and scan speed leads to higher porosity, greater surface roughness, and reduced hardness in the as-built condition, resulting in poorer corrosion performance. Specimens fabricated with a finer layer thickness (20 µm) exhibited substantially lower corrosion rates than those produced with thicker layers (60 µm), confirming the strong influence of DMLS processing parameters on corrosion behaviour. Shot peening significantly improved surface integrity by reducing surface defects and introducing compressive residual stresses, which enhanced corrosion resistance. The corrosion rate decreased by up to 77%, from 0.67 mm/y in the as-built condition to 0.15 mm/y after shot peening. Among the investigated conditions, specimens fabricated with 20 µm layer thickness and 100 mm/s scan speed followed by shot peening exhibited the most favourable combination of properties, including the lowest corrosion rate and improved surface integrity. These findings demonstrate that shot peening is an effective post-processing technique for improving the durability of DMLS-fabricated Cu–Ni alloys for marine and chemically aggressive applications.

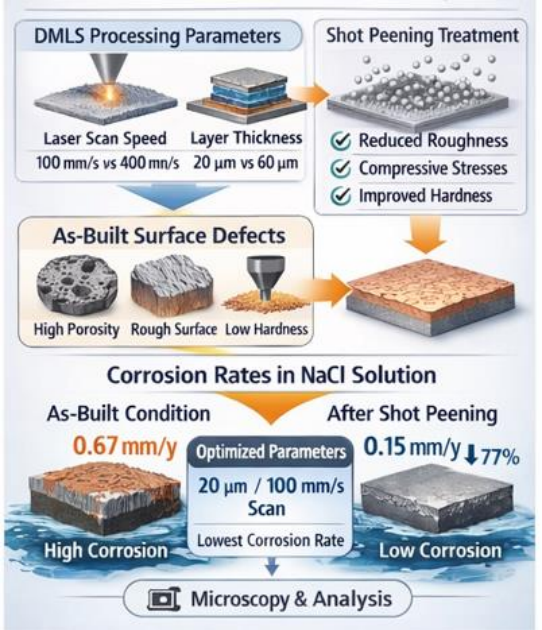

Keywords: DMLS; Cu–Ni Alloy; Shot Peening; Corrosion Resistance; Residual Stress, Surface Roughness, Additive Manufacturing.

Introduction

Additive manufacturing (AM) has transformed the fabrication of metallic components, enabling the production of complex geometries with tailored microstructures that are difficult to achieve through conventional processing routes [1]. Among AM techniques, laser powder-bed fusion (LPBF) and specifically Direct Metal Laser Sintering (DMLS) has gained prominence for producing near-net-shape metallic parts with high dimensional accuracy and improved material efficiency compared with subtractive manufacturing [2–4]. However, the layer-wise solidification inherent to DMLS introduces defects such as porosity, partially melted particles, and rough surfaces that can compromise mechanical integrity and corrosion resistance, particularly in aggressive service environments [5–9].

Copper-nickel (Cu–Ni) alloys occupy a critical role in marine, desalination, and chemical process industries owing to their inherent resistance to chloride-induced corrosion and their stable mechanical properties in aggressive aqueous environments [10,11]. While DMLS offers an attractive route to fabricating Cu–Ni components with complex geometries, the rapid solidification, surface-connected porosity, and tensile residual stresses generated during layer-wise processing significantly degrade the corrosion resistance that makes these alloys industrially valuable. These process-induced defects accelerate chloride ion ingress and localised corrosion initiation, undermining long-term component durability [10,11].

In particular, the tensile residual stresses generated during rapid DMLS solidification render the alloy susceptible to stress

1 Department of Mechanical Engineering, Global Academy of Technology, Autonomous Institute under Visvesvaraya Technological University, Karnataka, India. E-mail: rajesh.r@gat.ac.in; ORCID Id: 0000-0002-3146-4057
2 Department of Engineering and Technology, College of Engineering and Technology, University of Technology and Applied Sciences, Salalah, Sultanate of Oman.
3 Department of Chemistry, BMS Institute of Technology & Management, Autonomous Institute under Visvesvaraya Technological University, Karnataka, India. E-mail: bincypraveen@bmsit.in; ORCID Id: 0000-0001-8972-087X
4 Department of Mechanical Engineering, Sambhram Institute of Technology, Visvesvaraya Technological University, Karnataka, India. E-mail: psampathkumar29@yahoo.com; ORCID Id:0000-0002-4683-6626
5 Department of Mechanical Engineering, Indian Institute of Information Technology, Design and Manufacturing, Kurnool, India. E-mail: anand.subramaniyan@iiitk.ac.in; ORCID Id: 0000-0002-0877-3775
*Corresponding Author E-mail: Mithun.Kulkarni@utas.edu.om; Orchid Id: 0000-0001-5418-0148

corrosion cracking (SCC) in chloride environments, while surface-connected porosity creates occluded micro-cells where local pH decreases and chloride concentration increases — conditions that dramatically accelerate pit initiation and anodic dissolution [8,9]. These mechanisms make post-processing surface treatment essential to restore and enhance the intrinsic corrosion resistance of Cu–Ni alloys fabricated by DMLS.

Shot peening (SP) is a well-established mechanical surface treatment in which repeated high-velocity impacts induce severe plastic deformation, introducing compressive residual stresses, closing surface porosity, and refining the near-surface microstructure. These effects collectively improve fatigue life, wear resistance, and corrosion performance [12–14]. In conventionally manufactured alloys, SP has been shown to reduce surface roughness (Ra) significantly: AlMangour and Yang [15] reported a 28% reduction in Ra for shot-peened DMLS 17-4 stainless steel, while Calignano et al. [16] demonstrated that SP reduced Ra from approximately 14 µm to below 8 µm in DMLS aluminium parts. Maamoun et al. [17] found that SP of AM AlSi10Mg reduced Ra by around 40% and simultaneously increased surface hardness by over 20%. For copper-based systems, Gholami et al. [18] showed that SP of CuNi3SiMg alloys improved surface hardness and grain boundary density, enhancing corrosion resistance in chloride environments, while Lv et al. [19] reported reduced corrosion rates in shot-peened Ni–Al bronze alloys exposed to 3.5% NaCl. In the context of AM alloys more broadly, Żebrowski et al. [20] confirmed that SP of DMLS Ti-6Al-4V produced superior corrosion resistance compared with the as-built condition, and Mythreyi et al. [21] demonstrated that SP of SLM IN718 improved both hardness and corrosion resistance through microstructural refinement. These studies consistently show that SP improves surface roughness, hardness, residual stress state, and corrosion resistance across diverse alloy systems - yet the quantitative relationship between DMLS process parameters, SP-induced surface modification, and corrosion performance remains uncharacterised for Cu–Ni alloys. No prior study has systematically linked scan speed and layer thickness to post-SP corrosion outcomes in DMLS-fabricated Cu–Ni components. While existing studies treat either the build process or the surface treatment in isolation, none critically evaluates their combined and interactive effect on corrosion performance in Cu–Ni alloys. This constitutes a critical and unaddressed gap in the literature, given the growing demand for reliable Cu–Ni parts produced by AM for marine and aggressive-environment applications.

The present study addresses this gap by systematically investigating the combined effect of DMLS processing parameters (laser scan speed: 100–300 mm/s; layer thickness: 20–60 µm) and shot peening post-treatment on the porosity, surface roughness, microhardness, residual stress, and corrosion rate of DMLS-fabricated Cu–Ni alloys across nine parameter combinations. The scientific novelty of this work is distinguished from prior studies on three specific grounds: (i) first parametric study: no previous work has systematically mapped the combined effect of DMLS scan speed and layer thickness on post-SP corrosion performance in Cu–Ni alloys, and this parametric map is established here for the first time; (ii) quantified improvement: the degree of improvement in all five surface integrity metrics is established as a function of both build condition and SP, enabling evidence-based selection of processing parameters for a target performance level; and (iii) mechanistic understanding: the chain linking SP-induced surface-connected pore closure, near-surface grain refinement, and compressive residual stress introduction to measurable corrosion rate reductions is validated by SEM and EDS evidence, providing physical understanding beyond simple empirical correlation. It is hypothesised that specimens fabricated at lower scan speeds and thinner layer thicknesses will exhibit superior surface integrity and corrosion resistance in both as-built and shot-peened states, and that shot peening will provide the greatest absolute improvement in corrosion resistance for specimens with the lowest as-built defect density.

Materials and Experimental Procedure

Materials and DMLS Processing Parameters

Copper–nickel (Cu–Ni) alloy specimens were fabricated using the Direct Metal Laser Sintering (DMLS) process. A commercially available DM-20 powder supplied by EOS GmbH, Germany, was used as the feedstock material. The powder had an average particle size of approximately 20 µm and a nominal chemical composition of Cu 76.6 wt.%, Ni 14.6 wt.%, Sn 6.7 wt.%, and P 1.6 wt.%, according to the supplier specification. The presence of Tin(Sn) is known to improve corrosion resistance in Cu-based alloys by stabilising the passive oxide film and reducing anodic dissolution rates in chloride environments. Phosphorus (P) acts primarily as a deoxidiser during sintering and may influence the chemistry and continuity of the oxide layer at melt pool boundaries[22–25]. Since the alloy composition was fixed and identical across all nine build conditions, these elemental contributions affect the absolute corrosion performance of the alloy system but do not confound the comparative trends observed across processing conditions in this study.

Referring to Table 1, Cu–Ni specimens with dimensions of 10 mm in diameter and 4 mm in height were fabricated using an EOSINT M250 DMLS system (EOS GmbH, Germany). The build chamber was purged and maintained under a nitrogen inert atmosphere (oxygen content <0.1%) throughout the entire build process to prevent oxidation of the copper-rich powder and suppress the formation of oxide inclusions at melt pool boundaries [18]. The laser power was set to 240 W, delivered by a CO_2 laser operating at a wavelength of 10.6 µm [18]. The build platform was preheated to 80 °C prior to and maintained at this temperature throughout fabrication to reduce thermal gradients between successive layers, minimise residual stress accumulation, and promote inter-layer bonding. The build chamber ambient temperature was held at 25 ± 2 °C. A meander (alternating stripe) scan strategy was employed, with the scan direction rotated by 67° between successive layers to reduce anisotropy and promote a more uniform residual stress distribution in the as-built specimens. Layer thicknesses of 20, 40, and 60 µm were selected to span the range commonly reported for copper-alloy DMLS processing, where 20 µm represents a fine-resolution regime associated with high energy density and low porosity, and 60 µm represents a coarser regime that reduces build time but increases the risk of incomplete fusion and defect formation [3,4]. Scan speeds of 100, 200, and 300 mm/s were chosen to systematically vary the volumetric energy density delivered to the melt pool: 100 mm/s provides sufficient energy for near-complete powder melting, while 300 mm/s approaches the threshold at which lack-of-fusion porosity and surface balling become pronounced in this alloy system [3,5]. Together, the nine parameter combinations (three layer thicknesses × three scan speeds) provide a structured experimental matrix that allows the independent and interactive effects of these two most influential DMLS variables to be evaluated. The hatch spacing and beam diameter were fixed at 0.2 mm and 0.4 mm for all specimens so that the effect of the selected variables could be assessed without changing the remaining processing conditions.

Table (1): DMLS processing parameters used for fabrication of Cu–Ni alloy specimens. Fixed parameters were held constant across all nine conditions; variable parameters were systematically varied (3 layer thicknesses × 3 scan speeds = 9 conditions).

Parameter	Value	Basis for selection
Peening medium	Spherical alumina beads	Hardness, chemical stability, uniform energy transfer
Media diameter	0.1 mm	Equipment specification
Almen intensity	0.11 mmA (SAE J443)	Optimised over 5 levels (0.05–0.18 mmA); best Ra without cracking
Operating pressure	1 bar	Equipment specification
Treatment duration	60 s	Equipment specification
Nozzle stand-off	100 mm	Fixed for uniform coverage
Impact angle	90°	Maximises normal force; uniform compressive stress
Coverage	100% (visually verified)	Ensures uniform surface exposure

Table (2): Shot peening process parameters applied uniformly to all DMLS-fabricated Cu–Ni specimens. Parameters were selected following a structured pilot optimisation study conducted on sacrificial specimens prior to the main experimental campaign.

Parameter	Value / Range	Notes
DMLS system	EOSINT M250 (EOS GmbH)	
Laser type/wavelength	CO_2, 10.6 µm	
Laser power	240 W	Fixed
Scan speed	100, 200, 300 mm/s	Variable
Layer thickness	20, 40, 60 µm	Variable
Hatch spacing	0.2 mm	Fixed
Beam diameter	0.4 mm	Fixed
Scan strategy	Meander, 67° rotation	Fixed
Atmosphere	Nitrogen (O_2 < 0.1%)	Fixed
Build platform preheat	80 °C	Fixed
Chamber temperature	25 ± 2 °C	Fixed

After fabrication, the specimens were detached from the build platform by electrical discharge machining (EDM) and prepared for subsequent surface treatment and characterization. The selected processing window was intended to examine the influence of DMLS build parameters on porosity, surface condition, mechanical response, and corrosion behaviour of the fabricated Cu–Ni alloy specimens.

Shot Peening Process

Shot peening was applied as a mechanical surface treatment to improve the integrity of DMLS-fabricated Cu–Ni specimens. The surface was modified by accelerating abrasive particles through a nozzle. These particles struck the specimen repeatedly, and localized plastic deformation was induced. A schematic of the shot peening setup is shown in Figure 1.

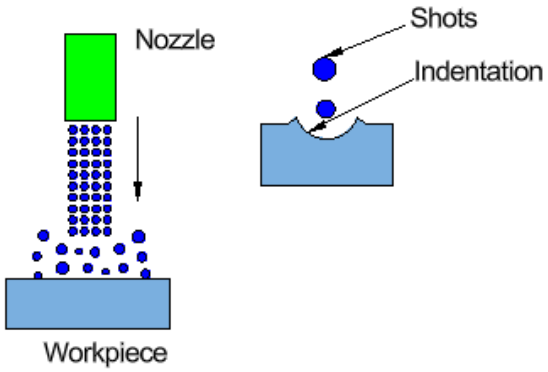

Figure (1): Schematic illustration of the shot peening setup used for surface treatment of DMLS-fabricated Cu–Ni specimens.

Spherical alumina beads were selected as the peening medium owing to their hardness, chemical stability, and ability to transfer impact energy uniformly, while minimising excessive surface damage.

The shot peening parameters were determined through a structured pilot optimisation study conducted on sacrificial Cu–Ni specimens fabricated under the same DMLS conditions as the main experimental campaign. In this pilot study, Almen intensity was systematically varied across five levels 0.05, 0.08, 0.11, 0.14, and 0.18 mmA (SAE J443), while all other parameters were held constant. After peening at each intensity level, surface roughness (Ra) was measured by profilometry, and the surface was examined optically for cracking, over-peening artefacts, and mechanical damage. The selection criterion was the intensity that produced the greatest reduction in Ra relative to the as-built surface without introducing any surface damage. An Almen intensity of 0.11 mmA satisfied this criterion and was therefore adopted for all specimens in the main campaign. All remaining parameters viz., operating pressure, nozzle stand-off distance, impact angle, treatment duration, and coverage were fixed based on equipment specifications and established practice in the literature for similar alloy systems. The finalised shot peening parameters are summarised in Table 2.

Experimental Characterization

Porosity Measurement

Porosity of the DMLS-fabricated Cu–Ni specimens was evaluated by comparing the experimentally measured density with the theoretical density calculated using the rule of mixtures. This approach is widely adopted for multi-component alloy systems to estimate volumetric porosity in additively manufactured materials. It should be noted that density-based porosity measurement, while practical and consistent with ASTM B311, does not capture pore morphology, spatial distribution, connectivity, or surface-connectivity all of which can independently influence corrosion behaviour. The absence of image-based validation (e.g., optical cross-sectional analysis, SEM, or X-ray computed tomography) is acknowledged as a limitation of the current study, and microstructural cross-sectional characterisation is recommended in future work for a more complete assessment of pore structure. The theoretical density (ρ_t = 8.42 g/cm³) was calculated based on the weighted densities of the constituent elements (Cu, Ni, Sn, and P), while the experimental density (ρ_e) was determined from direct mass and volume measurements of the specimens.

The mass of each specimen was measured using a calibrated Sartorius MCE36P-3S00-D HWL Cubis II High-Capacity micro balance with a readability of 0.0001 g. Prior to measurement, the samples were carefully cleaned using ethanol to remove any loosely adhered powder particles, ensuring

accurate mass determination. The volume of the cylindrical specimens was calculated using measured dimensions (diameter and height), obtained using a digital micrometre with an accuracy of ±0.01 mm. To minimize measurement variability due to geometric irregularities, dimensions were recorded at multiple locations and averaged.

The experimental density was calculated as the ratio of measured mass to calculated volume. The theoretical density and porosity were then determined using Equations (1) and (2), respectively:

$$\rho_t = \frac{100}{\sum_{i=1}^{n} \frac{x_i}{\rho_i}} \quad (1)$$

$$\%\text{Porosity} = \frac{(\rho_t - \rho_e)}{\rho_t} \times 100 \quad (2)$$

where ρ_t is the theoretical density, ρ_e is the experimentally measured density (g/cm³), and $x_i$and $\rho_i$represent the weight fraction and density of the constituent elements, respectively.

Potential sources of error in porosity estimation include surface roughness and geometric deviations inherent to the DMLS process, residual powder adhesion affecting mass measurement, and instrumental limitations in dimensional measurement. To mitigate these effects, samples were thoroughly cleaned prior to weighing, multiple dimensional readings were taken and averaged, and high-precision calibrated instruments were used. Although the density-based method does not distinguish between open and closed porosity, it provides a reliable estimate of overall volumetric porosity. This approach is consistent with ASTM B311 practices for density determination of metallic materials.[26,27].

Surface Roughness and Hardness Measurement

Surface roughness was measured on the top flat surface of the cylindrical specimens (perpendicular to the build direction), both before and after shot peening. In powder bed fusion–based additive manufacturing processes such as Direct Metal Laser Sintering (DMLS), surface morphology is strongly influenced by build orientation due to the layer-by-layer deposition mechanism. Surfaces inclined or parallel to the build direction generally exhibit higher roughness due to the staircase effect and surface irregularities associated with partially fused powder particles and melt pool instability during solidification [28,29]. In contrast, surfaces perpendicular to the build direction correspond to the final deposited layer and typically exhibit comparatively smoother morphology due to more uniform melt pool solidification during laser scanning [3,30,31]. This orientation-dependent variation in roughness has been widely reported in powder bed fusion processes [29,32].

The selected top surface represents the final deposited layer and directly reflects the influence of processing parameters such as scan speed and layer thickness. Since corrosion testing in this study was also performed on this surface, measuring roughness at the same location ensures that the surface interacting with the corrosive environment is accurately characterised, enabling a direct correlation between surface condition, shot peening treatment, and corrosion behaviour. This is particularly important because surface irregularities can act as preferential sites for localized corrosion initiation by promoting electrolyte retention and micro-galvanic interactions.

The curved lateral and bottom surfaces were excluded from roughness measurements. The lateral surface typically exhibits significantly higher roughness due to its geometric orientation and layer-wise deposition characteristics, which may not accurately represent the intrinsic surface condition and can lead to higher apparent roughness values. In addition, the curvature of the cylindrical surface may introduce inaccuracies in stylus-based profilometry. The bottom surface, which is detached from the build plate after fabrication, undergoes a different thermal history due to substrate contact and therefore does not represent the intrinsic as-built condition. As all specimens were fabricated with identical build orientation and geometry, these orientation-related effects remain constant, allowing reliable comparison of processing parameters and shot peening effects.

Surface roughness (Ra) was measured using a Mitutoyo SJ-210 surface profilometer in accordance with ISO 4287 and ISO 4288 standards. Measurements were performed at a traverse speed of 0.5 mm/s, and four readings were recorded at different locations on the selected surface. The reported Ra value represents the average of these measurements. The measurement uncertainty was within ±1%, indicating good repeatability of the roughness measurements.

Surface hardness was evaluated on the same top surface to ensure that the hardness values correspond directly to the surface affected by both the DMLS fabrication process and the shot peening treatment. Hardness measurements were performed using the Vickers microhardness method in accordance with ASTM E384, employing a VH1102 hardness tester equipped with a diamond indenter. An applied load of 1 kgf (HV1) with a dwell time of 15 s was used.

Five indentations were made at different locations on each specimen. To ensure independent measurements the spacing between adjacent indentations was maintained at approximately 500–1000 µm. This satisfies the requirement of ASTM E384, which recommends a minimum spacing of at least 2.5 times the indentation diagonal length. The reported hardness value represents the average of the five measurements. The variation between readings was within ±1 VHN, indicating consistent hardness response across the measured surface.

Residual Stress Measurement

Residual stress measurements were performed using X-ray diffraction (XRD) based on the sin²ψ method, following the procedure outlined in ASTM E2860-13. This method utilizes the crystal lattice spacing as an internal strain gauge, whereby residual stresses cause measurable shifts in the Bragg diffraction angle [33,34]. The sin²ψ method is well-established for surface residual stress determination in metallic alloys and is consistent with procedures described by Withers and Bhadeshia [34], Noyan and Cohen [35,36], and the NPL Good Practice Guide for X-ray Diffraction Residual Stress Measurement [37]. These references provide established methodological support for the measurement procedure, instrumentation, and data analysis approach employed in this study.

A chromium radiation source (Cr-Kα, λ = 2.2909 Å) was employed, operating at an accelerating voltage of 20 kV and a tube current of 4 mA. The tilt angle (ψ) was varied from 0° to 45° in increments of 5°, yielding nine ψ-angles per measurement location. The shift in diffraction peak position (Δ2θ) was recorded at each ψ-tilt, and the residual stress (σ) was calculated from the slope of the Δ2θ vs. sin²ψ plot using the relationship shown in Eq. (3) [33,38]:

$$\sigma = \frac{E}{2\nu} \cdot \frac{\partial(2\theta)}{\partial(Sin^2\psi)} \quad (3)$$

where E is the Young's modulus and v is the Poisson's ratio of the material. X-ray elastic constants consistent with published values for the material under investigation were used in the calculation [35].

The linearity of the Δ2θ versus sin²ψ plots was verified for all measurements, confirming the validity of the applied method and the absence of significant measurement artefacts. To account

for possible spatial variability arising from microstructural heterogeneities and surface condition differences [34,37], four independent measurements were performed at distributed locations across the surface of each specimen. The reported residual stress represents the mean of these measurements, and the relatively low variation between readings indicates good repeatability and reliability of the technique, ensuring that the measured values are representative of the overall surface stress state.

To support the validity and physical plausibility of the measurement approach, the residual stress values obtained in this study are compared with independently reported literature values. The compressive residual stress magnitudes measured after shot peening (up to −155 MPa) are consistent with values reported for comparable peening conditions in additively manufactured alloys: Żebrowski et al.[20] reported post-SP residual stresses in the range of −120 to −180 MPa for DMLS Ti-6Al-4V processed under similar Almen intensities, and Shen et al. [39] reported comparable compressive stress magnitudes following laser shock peening of Ti-6Al-7Nb alloys. The as-built compressive near-surface stresses measured in this study (−35 to −100 MPa) are similarly consistent with the range reported by Mugwagwa et al. [8] for AM alloys processed under comparable layer-wise solidification conditions. This agreement supports the physical plausibility and validity of the measurement approach employed in this study.

It should be noted that X-ray diffraction based residual stress measurement is inherently surface-sensitive, with a typical penetration depth of approximately 10–15 μm for the Cr-Kα radiation used in this study. Therefore, the reported values represent near-surface residual stresses rather than bulk stress distribution. This is particularly relevant for shot-peened specimens, where residual stress gradients are expected, typically transitioning from compressive stresses at the surface to less compressive or tensile stresses in the subsurface region. However, since corrosion processes are primarily governed by surface and near-surface conditions, the measured residual stress values remain highly relevant for evaluating the influence of shot peening on corrosion behaviour.

Surface Topology and Microstructural Examination

Surface morphology and topographical features were examined using scanning electron microscopy (SEM). Elemental composition was identified by energy-dispersive X-ray spectroscopy (EDS). These observations were used to study surface deformation, corrosion-affected regions, and compositional changes caused by exposure.

Porosity distribution was evaluated from optical micrographs. Image-analysis methods were applied in accordance with metallographic preparation and examination procedures outlined in ASTM E3 and ASTM E407. This ensured that porosity assessment was consistent and reliable across all specimens.

Corrosion Rate Measurement

The corrosion behaviour of the AM samples before and after the shot peening (SP) process was evaluated under brackish water conditions using a 3% sodium chloride solution, in accordance with ASTM G31. Prior to testing, the specimens were cleaned with acetone and air-dried to remove surface contaminants. The initial masses of the specimens were recorded using a calibrated Sartorius MCE36P-3S00-D Cubis II high-capacity microbalance with a readability of 0.0001 g, ensuring high precision in mass measurement.

The test solution was prepared by dissolving 3 g of sodium chloride in 100 mL of deionized water to obtain a 3% NaCl solution representative of brackish water conditions. Two specimens per condition were immersed in the solution at room temperature for a total exposure duration of 720 h. While two specimens were used for each condition, the reliability of the results was ensured through repeated interval-based measurements over the exposure period, providing multiple data points per specimen.

To maintain the stability of the test environment, the NaCl solution was renewed every 7 days during the exposure period to prevent depletion of chloride ions and accumulation of corrosion products, in line with recommended practices for long-duration immersion testing.

Weight loss measurements were recorded at regular intervals of 72 h, yielding ten measurement points per specimen over the 720 h exposure period. This repeated-measurement approach enhances the reliability of corrosion rate determination by capturing the progression of mass loss over time, rather than relying on a single end-point measurement.

At each interval, specimens were removed, rinsed with distilled water to eliminate loose corrosion products, cleaned with ethanol, and dried in a hot air oven at 60 °C for 30 min. The specimens were then cooled in a desiccator prior to weighing to prevent moisture re-adsorption and ensure consistent mass measurement.

The percentage weight loss was calculated using Eq. (4), and the corrosion rate was determined using Eq. (5):

$$\text{Percentage weight loss} = \frac{W_1 - W_2}{W_1} \times 100 \quad (4)$$

$$\text{Corrosion rate (mm/y)} = \frac{8.76 \times 10^4 \, W}{D \, A \, T} \quad (5)$$

where $W_1$is the initial mass (g), $W_2$is the final mass (g), W is the weight loss (g), A is the exposed surface area (cm^2), T is the exposure time (h), and $D$is the material density (g/cm^3).

The corrosion rate for each condition was determined from the average of the interval-based measurements, ensuring that the reported values reflect consistent corrosion behaviour over the entire exposure period. In addition, both specimens within each condition exhibited consistent corrosion trends, indicating good repeatability of the experimental procedure.

Results and Discussion

Table 3 summarizes the alloy designation, DMLS processing parameters, and the measured values of porosity, hardness, surface roughness, and residual stress for the Cu–Ni alloy specimens before and after shot peening. The results show that both the DMLS processing conditions and the post-processing treatment strongly influenced the surface integrity and corrosion behaviour of the fabricated samples. In Table 3, the uncertainty values reported for porosity (e.g., ±0.03–0.05%) represent the propagated instrument precision derived from the balance readability (±0.0001 g) and digital micrometre accuracy (±0.01 mm), rather than statistical standard deviations from repeat measurements. The uncertainty values reported for residual stress (e.g., ±7-18 MPa) represent the XRD fitting uncertainty from the $\sin^2\psi$ regression, consistent with the methodology described by Withers and Bhadeshia [34] and Fitzpatrick et al. [37]. Hardness values are reported as the average of five measurements; the variation between readings was within ±1 VHN for all specimens, indicating good measurement consistency. These uncertainty values are reported in the table to reflect the precision of each measurement technique rather than statistical variability across specimens, and this distinction is explicitly acknowledged as a limitation associated with the

restricted sample size (n = 2 per condition) discussed in the corrosion testing section.

Effect of Process Parameters on the As-Built Condition

The manufacturing parameters in DMLS, particularly layer thickness and scan speed, significantly affect the porosity, surface roughness, and hardness of fabricated Cu–Ni alloy samples prior to shot peening. As shown in Table 3, increasing layer thickness from 20 µm to 60 µm and increasing scan speed from 100 mm/s to 300 mm/s results in higher porosity, increased surface roughness, and reduced hardness. This trend is attributable to lower input energy per unit volume, which leads to incomplete powder melting, balling, and lack-of-fusion defects.

The bulk (volumetric) porosity values reported in Table 3 are considered relevant to corrosion performance based on the mechanistic reasoning that higher bulk porosity, as observed in specimens fabricated at greater scan speeds and layer thicknesses, is likely associated with a larger internal surface area accessible to the 3% NaCl solution via surface connected channels. This is expected to increase the effective electrochemically active area beyond the nominal geometric surface, accelerating anodic dissolution and promoting occluded-cell corrosion within pore interiors where oxygen depletion and chloride accumulation further drive localised attack. It must be acknowledged, however, that this porosity–corrosion relationship is supported by mechanistic reasoning and corroborated by the SEM evidence of reduced pit density after SP (Fig. 3), rather than by direct experimental mapping of pore connectivity before and after shot peening. The density-based porosity measurements used in this study do not provide information on pore geometry, surface-connectivity, or the degree to which pores are closed by SP. X-ray computed tomography or detailed cross-sectional SEM imaging before and after SP is recommended in future work to directly validate this correlation. [7,10,11]. The positive correlation between porosity and corrosion rate observed across all nine conditions in Table 4 is therefore a direct consequence of this mechanism: specimens with lower bulk porosity (e.g., sample 120: 3.7%) exhibit the lowest corrosion rates (0.67 mm/y as-built), while those with higher porosity (e.g., sample 360: 7.2%) show the highest corrosion rates (1.74 mm/y as-built), confirming that bulk porosity is a key determinant of corrosion performance in DMLS-fabricated Cu–Ni alloys.

The optical micrographs compiled in Figure 2(a–h) visually corroborate these quantitative trends. As-built samples with lower thickness and slower scan speed (e.g., Fig. 2(a,c)) show comparatively fewer dark voids and discontinuities, whereas higher-thickness and higher-speed counterparts (e.g., Fig. 2(e,g)) exhibit a higher density of pores and micro-voids.

These trends are consistent with established DMLS behaviour reported across multiple alloy systems [16,17,40,40–44]. The as-built characterisation presented here serves primarily as a necessary baseline against which the effect of shot peening is quantified; the primary focus of the subsequent discussion is the improvement in surface integrity and corrosion resistance attributable to shot peening.

Effect of Shot Peening on Surface Integrity

Shot peening produces consistent and measurable improvements in surface integrity across all nine Cu–Ni parameter conditions. As summarised in Table 3, surface roughness (Ra) decreased by 25–36% across all conditions, hardness increased by 15–30%, and compressive residual stress magnitudes increased by 40–55 MPa relative to the as-built state. These improvements are visually confirmed in the optical micrographs of Figure 2(b,d,f,h), where shot-peened surfaces show fewer surface-connected pores, smoother textures, and evidence of plastic deformation compared with their as-built counterparts in Figure 2(a,c,e,g).

This leads to closure of surface-connected defects, grain refinement near the surface, and the development of compressive residual stresses that strengthen the surface layer. Similar improvements in surface hardness, roughness, and residual stress state after shot peening have been widely reported in several alloy systems [17,21,40,43,44].

Importantly, for Cu-based alloys, intrinsic processing challenges such as high thermal conductivity and rapid solidification often result in elevated porosity and surface defects in as-built AM parts [45].

The surface roughness reductions observed in the present study (25–36% across all conditions) are consistent with, and in good agreement with, values reported in the literature for SP of DMLS and AM alloys. AlMangour and Yang [16] reported a Ra reduction of approximately 28% in shot-peened DMLS 17-4 stainless steel using alumina media at comparable Almen intensities, while Calignano et al. [16] demonstrated that SP reduced Ra from approximately 14 µm to below 8 µm (a 43% reduction) in DMLS aluminium parts with higher initial roughness. Maamoun et al. [17] achieved a Ra reduction of approximately 40% in SP of AM AlSi10Mg parts. The present Ra reductions of 36% (sample 120: from 6.1 to 3.9 µm) to 25% (sample 360: from 12.3 to 9.3 µm) fall within this reported range and confirm that the SP conditions used in this study are appropriate for surface roughness improvement in DMLS copper-based alloys. Notably, the absolute post-SP Ra values achieved for the best-performing condition (3.9 µm for sample 120) are comparable to values reported by AlMangour and Yang [15] for shot-peened DMLS 17-4 SS (approximately 3.5–4.5 µm), supporting the validity of the SP parameters selected. The slightly lower percentage reductions observed at higher scan speeds and layer thicknesses in the present study (25–30%) compared with the best conditions (33–36%) are attributable to the higher initial Ra values, which require greater plastic deformation to smooth the surface asperities a trend also observed by Calignano et al. [16] for higher-roughness DMLS surfaces.

Table 3: Density, Porosity, experimental density, hardness, surface roughness, and residual stress of DMLS-fabricated Cu–Ni alloys before and after shot peening

Alloy No.	Laser scan speed (mm/s)	Layer thickness (μm)	Density (g/cm³) (ρ_e)	Porosity (%)	Hardness (VHN)		Surface Roughness (Ra), μm		Residual Stress (MPa)	
					Before Shot Peening	After Shot Peening	Before Shot Peening	After Shot Peening	Before Shot Peening	After Shot Peening
120	100	20	8.11 ± 0.03	3.7	146	163	6.1	3.9	-100±18	-155±11
220	200		7.89 ± 0.04	6.3	111	129	8.5	4.8	-83±10	-136±8
320	300		7.87 ± 0.05	6.5	79	97	9.1	6.1	-65±9	-111±7
140	100	40	8.02 ± 0.03	4.8	96	114	8.2	4.6	-71±15	-124±18
240	200		7.84 ± 0.04	6.9	78	97	9.9	6.3	-57±10	-105±12
340	300		7.82 ± 0.05	7.1	66	86	10.7	8.1	-45±10	-96±13
160	100	60	7.99 ± 0.03	5.1	91	111	10.1	7.3	-47±11	-107±12
260	200		7.83 ± 0.04	7.0	75	97	11.2	8.6	-39±8	-88±7
360	300		7.81 ± 0.05	7.2	65	85	12.3	9.3	-35±8	-79±9

Kindly Note: Density and residual stress values are reported as mean ± uncertainty. Hardness values represent the average of five indentations (n = 5), and surface roughness (Ra) values represent the average of four measurements (n = 4). Due to experimental constraints, standard deviation is not reported; however, measurement variability was within ±1 VHN for hardness and ±1% for surface roughness.

Microstructural Evidence of Surface-Connected Porosity Closure

It is important to note that shot peening is a surface treatment; it does not alter the bulk (volumetric) internal porosity of the specimens, which is governed exclusively by the DMLS processing parameters. The discussion in this section therefore refers specifically to surface-connected porosity pores that intersect or communicate with the specimen surface and are visible in the top-surface optical micrographs. The optical micrographs in Figure 2 provide direct microstructural evidence that shot peening physically closes surface-connected pores visible at the specimen surface. The reduction in dark regions associated with surface-connected micro-voids after peening confirms that plastic deformation from shot peening collapses near-surface pores and enhances local densification, thereby improving surface integrity and reducing the number of sites available for electrolyte ingress.

The interpretation agrees with findings in additive manufacturing literature. Studies on metallic powders subjected to post-processing show that higher peening closes interconnected porosity. This occurs because plastic flow and work hardening are promoted in the surface layer. In copper-rich alloys, where porosity is common due to rapid thermal gradients and high thermal conductivity, such treatments are especially beneficial [45].

These micrographs confirm that shot peening produces measurable improvements in surface hardness and roughness across all conditions, with the most pronounced changes observed in specimens fabricated at the lowest scan speed and thinnest layer thickness (samples 120 and 140). The visual reduction in dark surface-connected voids after peening is consistent with near-surface plastic deformation closing pores that communicate with the specimen surface, rather than any change to the bulk internal porosity, which is governed solely by the DMLS processing conditions.

Influence of Shot Peening on Residual Stress

Residual Stress Before Shot Peening

The residual stress values of the DMLS-fabricated Cu–Ni alloy samples obtained at different layer thicknesses and scan speeds are summarized in Table 3. Negative values indicate compressive residual stress. It is observed that compressive stress decreases in magnitude from approximately −100 MPa to −35 MPa as the scan speed increases from 100 mm/s to 300 mm/s, irrespective of layer thickness. The presence of compressive residual stresses in the as-built condition warrants explanation, as DMLS typically generates tensile residual stresses due to rapid solidification and large thermal gradients. In the present study, several factors are likely responsible for the observed compressive state: (i) the build platform was preheated to 80 °C, which reduces the thermal gradient between successive layers and moderates the tensile stress development typical of ambient-temperature DMLS builds; (ii) the 67° scan rotation strategy between successive layers promotes a more isotropic stress distribution, which may offset directional tensile accumulation; and (iii) the small specimen geometry (10 mm diameter × 4 mm height) facilitates greater stress redistribution compared to larger components. These factors are consistent with observations reported by Ali et al. [46] and Liu et al. [47], who demonstrated that preheat temperature and scan strategy significantly influence the sign and magnitude of residual stresses in LPBF alloys. Nevertheless, the absolute stress state of the as-built specimens warrants further investigation, and through-thickness profiling via neutron diffraction is recommended in future work.

The higher compressive stresses observed at lower scan speeds can be attributed to greater energy input and more uniform melting, which promotes improved metallurgical bonding and induces higher thermal gradients during solidification. The surface layers consistently exhibit higher compressive stresses than the subsurface, because the top layer cools more rapidly while the underlying material constrains contraction, thereby suppressing stress relaxation. Such stress gradients with scan speed may arise from localized plastic deformation, thermal contraction mismatch, and phase-transformation-induced strains during layer-by-layer solidification. Similar scan-speed-dependent residual stress trends in AM alloys were reported by Mugwagwa et al. [8], lending strong support to the present observations.

Layer thickness also plays a significant role in residual stress development. As shown in Table 3, samples produced using a 20 μm layer thickness exhibit compressive stresses in the range of −100 to −65 MPa, whereas samples fabricated at 60 μm thickness show lower compressive stresses between −47 and −35 MPa. Thus, thinner layers generate higher compressive residual stresses. This behaviour is consistent with the literature [47,48], which reports that thinner layers in additive manufacturing generally exhibit lower porosity, higher density, and greater resistance to elastic relaxation, thereby sustaining

higher compressive stresses. Therefore, prior to shot peening, both scan speed and layer thickness strongly influence the magnitude and distribution of residual stresses in DMLS-fabricated Cu–Ni alloys.

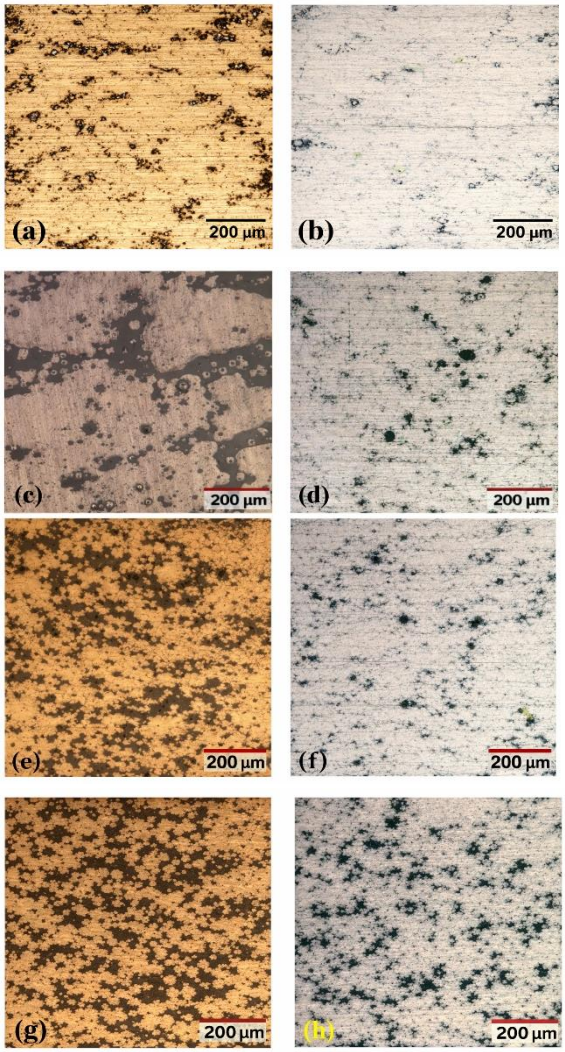

Figure (2): Optical micrographs of the top flat surface (build surface, perpendicular to the build direction) of DMLS-fabricated Cu–Ni alloy specimens, prepared by light surface polishing without cross-sectioning. Each row presents the same specimen before (left column: as-built condition) and after (right column: shot-peened condition): (a–b) Sample 120 (100 mm/s, 20 µm), (c–d) Sample 160 (100 mm/s, 60 µm), (e–f) Sample 320 (300 mm/s, 20 µm), and (g–h) Sample 360 (300 mm/s, 60 µm). Dark regions correspond to surface-connected pores and micro-voids.

Residual Stress After Shot Peening

After shot peening, the DMLS samples exhibit a substantial increase in compressive residual stress, as indicated in Table 3, although the overall trends with scan speed and layer thickness remain unchanged. Increasing either scan speed or layer thickness leads to a reduction in compressive stress magnitude, confirming that residual stress remains process-parameter dependent even after peening.

The enhancement of compressive residual stress after shot peening arises from localized plastic deformation induced by high-velocity alumina shot impacts. These impacts convert elastic deformation into permanent plastic strain, producing high dislocation densities, grain refinement, and lattice distortion near the surface. This process generates a deep compressive stress field, which improves resistance to crack initiation, fatigue, corrosion, and wear.

The combined influence of scan speed and layer thickness on residual stress evolution in AM parts has been reported previously , highlighting the critical role of compressive stress in determining mechanical and metallurgical performance. The present results are in strong agreement with these findings. Xiaojun Shen et al. [39] reported that laser shock peening (LSP) of Ti-6Al-7Nb alloys generated compressive residual stresses ranging from −42 MPa to −512 MPa, significantly delaying crack initiation. Similarly, Ahmed H. Maamoun et al. [17] observed an increase in compressive stress from −150 MPa to −170 MPa in shot-peened AlSi10Mg AM parts, with peening improving crack resistance at a depth of 90 µm. Bandar AlMangour et al. [15] reported compressive stresses as high as −700 MPa in shot-peened additively manufactured 17-4 stainless steel, attributed to crystallographic rearrangement and lattice distortion caused by severe plastic deformation. Furthermore, Bagherifard et al. [48] demonstrated that shot peening induces phase transformation from austenite to martensite in 316L stainless steel, thereby reducing crack propagation and enhancing surface durability.

Collectively, these studies confirm that shot-peening-induced compressive residual stresses are a dominant factor governing fatigue life, corrosion resistance, and wear behaviour through microstructural refinement, hardness enhancement, porosity closure, and surface densification. The present Cu–Ni alloy system exhibits similar beneficial responses, providing strong validation of the effectiveness of shot peening in optimizing residual stress and surface integrity in additively manufactured components [9,11,18,19,39,46,48–51].

Corrosion Damage Analysis Before and After Shot Peening

Corrosion behaviour of the DMLS-fabricated Cu–Ni alloy samples was evaluated using weight-loss measurements in 3% NaCl solution for a total duration of 720 h, simulating a marine environment. The corrosion rate and weight loss data for the 120–320, 140–340, and 160–360 sample sets are presented in Table 4. The results were analysed to determine the influence of scan speed and layer thickness on corrosion performance before and after shot peening. It is evident from Table 4 that shot peening significantly reduces both weight loss and corrosion rate across all processing conditions, indicating improved corrosion resistance.

It is acknowledged that weight-loss immersion testing provides cumulative mass loss over the full exposure period but does not yield real-time kinetic information or distinguish between uniform and localised corrosion mechanisms. It does not produce electrochemical parameters such as corrosion potential, passive current density, or pitting potential, which would provide complementary mechanistic insight. These limitations are recognised, and future work will incorporate potentiodynamic polarisation and electrochemical impedance spectroscopy (EIS) to characterise the electrochemical kinetics of DMLS-fabricated Cu–Ni alloys before and after shot peening, providing a more complete picture of the corrosion protection mechanism.

Corrosion Behaviour in As-Built (Before Shot Peening) Condition

The corrosion data prior to shot peening indicate a clear dependence on both scan speed and layer thickness. Among all samples, sample 120 (20 µm, 100 mm/s) exhibits the lowest corrosion rate, whereas sample 160 (60 µm, 100 mm/s) shows the highest corrosion rate, as seen in Table 4. The corrosion rate increases systematically with increasing scan speed and layer thickness across all groups, a trend that is directly interpretable in terms of increasing porosity and surface defect density at higher energy densities. The specific numerical values for each

condition are tabulated in Table 4 and are not restated here; the following discussion focuses on the mechanistic interpretation of these trends.

The deterioration in corrosion resistance with increasing scan speed and layer thickness is primarily associated with increased porosity, surface roughness, and reduced metallurgical continuity in the DMLS samples. Higher scan speeds reduce the effective energy input per unit volume, promoting partial melting, balling, and lack-of-fusion defects, while thicker layers require more energy for complete densification, leading to increased void formation. These microstructural defects act as preferential sites for chloride ion penetration and localized corrosion initiation.

This behaviour is consistent with the microstructural observations reported earlier in Fig. 2(a,c,e,g), where higher-thickness and higher-speed samples exhibit a higher density of surface-connected pores. Increased porosity not only increases the effective exposed surface area but also promotes the formation of occluded cells that accelerate electrochemical corrosion. Therefore, samples produced with lower scan speed (100 mm/s) and thinner layers (20 µm) demonstrate superior corrosion resistance due to lower porosity, smoother surfaces, and higher hardness, which together reduce electrolyte ingress and anodic dissolution.

Effect of Shot Peening on Corrosion Behaviour

Shot peening reduces the corrosion rate across all nine Cu–Ni conditions, with percentage improvements ranging from 52.8% (sample 360: 300 mm/s, 60 µm) to 77% (sample 120: 100 mm/s, 20 µm), as detailed in Table 4. As shown in Table 4, for the same layer thickness and scan speed, both weight loss and corrosion rate decrease after shot peening. The absolute reduction in corrosion rate ranges from 0.52 mm/y (sample 120: from 0.67 to 0.15 mm/y) to 0.92 mm/y (sample 360: from 1.74 to 0.82 mm/y). Although the relative ranking of conditions is preserved - lower scan speed and thinner layers continue to exhibit lower absolute corrosion rates after SP - the greatest percentage improvement (77%) is achieved in the best-performing as-built specimen (sample 120), where the already-dense microstructure provides an ideal substrate for SP-induced further densification and compressive stress introduction.

The enhanced corrosion resistance after shot peening is attributed to plastic deformation–induced densification, grain refinement, and compressive residual stress generation in the surface layer. Shot peening collapses surface-connected pores, smoothens asperities, and introduces compressive stresses that suppress pit initiation and crack opening, thereby reducing electrochemical activity at the surface.

The mechanistic chain governing this improvement can be stated explicitly: (i) SP-induced compressive residual stresses counteract the tensile stresses responsible for stress corrosion cracking (SCC) initiation at surface defects. By converting the near-surface stress state from tensile (as-built DMLS condition) to compressive (post-SP), the driving force for crack opening under chloride exposure is removed, suppressing SCC initiation and pit propagation. (ii) Surface-connected pore closure by SP reduces the internal surface area accessible to the NaCl electrolyte, eliminating occluded micro-cells where local pH drops, and chloride concentration builds up to levels that far exceed bulk solution chemistry. (iii) Near-surface grain refinement increases grain boundary density, distributing electrochemical activity more uniformly and reducing preferential anodic dissolution associated with coarse-grained as-built microstructures. Together, these three mechanisms act synergistically to produce the 52.8–77% corrosion rate reductions observed across all nine conditions, with the greatest benefit achieved where SP acts on the most defect-free starting microstructure (sample 120: 77% reduction). It is worth noting critically, however, that the absolute improvement delivered by SP was smaller for high-porosity specimens (e.g., samples 360 and 260 fabricated at 300 mm/s and 60 µm), where the as-built defect density may exceed the capacity of SP at the Almen intensity used here to fully close surface-connected pores. This suggests a practical ceiling on the effectiveness of SP as a remediation technique: when porosity is very high, SP alone is insufficient to fully restore corrosion performance to the level achievable from optimised build conditions, and pre-optimisation of DMLS parameters remains the primary lever for corrosion performance control. Furthermore, the reported porosity–corrosion correlation, while mechanistically logical and supported by SEM evidence, is based on density measurements rather than direct pore-connectivity mapping, and this indirect nature of the evidence should be acknowledged when interpreting the magnitude of SP-induced improvements.

These findings are strongly supported by existing literature. Iswanto et al. [11] demonstrated that shot peening of 316L stainless steel significantly reduced corrosion rate due to grain refinement and hardness increase. Żebrowski et al. [20] reported that shot-peened DMLS-fabricated Ti-6Al-4V alloys exhibited superior corrosion resistance compared to unpeened samples. Importantly for copper-based systems, Gholami et al. [18] showed that shot peening improved corrosion resistance in high-strength CuNi3SiMg alloys by increasing surface hardness and grain boundary density. Similarly, Lv et al. [19] reported that shot-peened Ni–Al bronze alloys in 3.5% NaCl exhibited reduced corrosion rates despite minor roughness changes. Mythreyi et al. [21] and Okuniewski et al. [52] further confirmed that shot peening improves corrosion resistance in AM alloys through microstructural refinement and residual stress modification.

Thus, the present Cu–Ni alloy system exhibits corrosion behaviour that is broadly consistent with established shot-peening mechanisms reported in both AM and copper-based alloys. However, it is important to note several points of nuance that qualify this comparison. First, the referenced studies involve different alloy systems (316L, Ti-6Al-4V, IN718, CuNi3SiMg), and direct quantitative comparison of SP-induced improvements across these systems must account for differences in base alloy corrosion resistance, porosity levels, and peening parameters. Second, while the combination of porosity reduction, surface densification, hardness enhancement, and compressive residual stress introduced by shot peening is identified as responsible for the corrosion rate reductions observed, the relative contribution of each mechanism cannot be independently quantified from the current dataset. Electrochemical testing (e.g., potentiodynamic polarisation, EIS) and direct pore-connectivity characterisation would be required to decouple these effects. Third, the as-built compressive residual stress state - atypical of DMLS - means that the beneficial stress state change induced by SP in this study may be smaller than in more conventional DMLS builds exhibiting tensile as-built stresses, and this should be considered when generalising the findings to other DMLS Cu–Ni processing conditions. Notwithstanding these qualifications, the consistent improvement across all nine parameter conditions provides robust evidence that shot peening is an effective post-processing technique for improving the durability of additively manufactured Cu–Ni components.

Corrosion Damage Assessment Using SEM

The scanning electron microscopy (SEM) images of the corroded Cu–Ni alloy samples 120, 160, 320 and 360 before and after shot peening are presented in Fig. 3(a–h), respectively.

These micrographs provide direct visual evidence of the surface degradation caused by chloride-induced corrosion and its modification by shot peening, thereby supporting the quantitative corrosion rate data presented earlier.

The SEM images of sample 120 before and after shot peening are shown in Fig. 3(a) and Fig. 3(b), respectively. The unpeened surface (Fig. 3a) exhibits pronounced corrosion features, including pits, micro-cracks and irregular corrosion deposits, which originate from the preferential attack of chloride ions at surface-connected pores and micro-defects. After shot peening (Fig. 3b), the surface appears significantly smoother and more compact, with markedly reduced pit density and surface damage. This improvement is attributed to the closure of surface porosity, plastic deformation induced densification, and reduction of surface roughness, which limit electrolyte penetration and suppress localized corrosion initiation. These observations are consistent with the lower corrosion rate and higher hardness measured for shot-peened samples.

Similar behaviour is observed for the other samples. The SEM images of samples 160, 320 and 360 shown in Fig. 3(c, e, g), respectively, demonstrate that the unpeened surfaces contain a higher density of corrosion pits, cracks, and loosely adhered corrosion products, while the corresponding shot-peened surfaces shown in Fig. 3(d, f, h) exhibit more uniform morphology with fewer corrosion features. These microstructural changes confirm that shot peening enhances corrosion resistance by reducing the number of electrochemically active sites and improving surface integrity, thereby providing strong microstructural validation for the corrosion rate trends observed in Table 4.

Table (4): Weight loss, corrosion rate, and percentage improvement of DMLS-fabricated Cu–Ni alloy samples with different layer thicknesses and scan speeds measured in 3% NaCl solution after 720 h exposure, before and after shot peening. Values represent the average of four independent measurements (n = 4).

Alloy Designation	Layer Thickness	Laser scan speed (mm/s)	Weight loss Percentage		Corrosion rate (mm/y)		Percentage improvement in corrosion rate (mm/y)
			Before Shot peening	After Shot peening	Before Shot peening	After Shot peening	
120	20 µm	100	0.72	0.44	0.67	0.15	77
220		200	2.10	0.86	0.92	0.26	72
320		300	3.09	1.03	1.39	0.41	71
140	40 µm	100	1.96	0.82	0.86	0.28	67.5
240		200	2.68	1.08	1.19	0.40	66.3
340		300	3.26	1.83	1.39	0.51	63.4
160	60 µm	100	2.09	1.08	1.07	0.36	66.3
260		200	3.94	1.67	1.42	0.73	58.4
360		300	4.15	2.75	1.74	0.82	52.8

EDX Analysis of Corrosion Products

To investigate the nature of the corrosion products formed after immersion in NaCl solution, EDX analysis was performed on the corroded surfaces before and after shot peening (SP). The SEM micrographs and the EDAX spectra shown in Fig. 4(a,b) correspond to the representative sample 360 and indicate the surface region selected for EDX examination in the unpeened and peened conditions.

It should be emphasized that Fig. 4 represents only sample 360, which was selected as the representative specimen from the 60 µm layer-thickness group fabricated at a scan speed of 300 mm/s. In contrast, Table 5 summarizes the EDX results for all investigated samples, including both 20 µm and 60 µm layer-thickness conditions. Therefore, the figures provide representative morphological and spectral evidence, whereas the table presents the elemental comparison for the full sample set.

EDX measurements were performed at multiple representative locations on each specimen to ensure consistency of compositional observations. Due to the localized nature of EDX analysis, the reported values are considered semi-quantitative and representative rather than statistical averages.

The SEM images mainly serve to identify the analysed region on the corroded surface before and after SP. The elemental changes are more clearly established through the EDX spectra and the quantitative results listed in Table 5. In all samples, the detected amounts of sodium (Na) and chlorine (Cl) decrease after shot peening. As these elements are associated with NaCl-derived corrosion deposits, their reduced presence after SP indicates that shot peening suppresses the accumulation or retention of corrosion products on the surface.

For the samples produced with a layer thickness of 20 µm, the Na content decreases from 11.2, 12.7, and 13.1 wt.% to 6.8, 7.5, and 7.9 wt.% for samples 120, 220, and 320, respectively. Over the same group, the Cl content decreases from 0.68, 0.71, and 0.84 wt.% to 0.28, 0.30, and 0.36 wt.%. A similar trend is observed for the 60 µm group. For samples 160, 260, and 360, the Na content decreases from 13.3, 13.9, and 14.3 wt.% to 8.0, 8.2, and 8.7 wt.%, respectively, while the Cl content decreases from 1.14, 1.67, and 2.00 wt.% to 0.46, 0.62, and 0.72 wt.%.

Among all conditions, sample 360 exhibits the highest Na and Cl contents before SP, namely 14.3 wt.% and 2.00 wt.%, respectively. After SP, these values decrease to 8.7 wt.% and 0.72 wt.%. This reduction is consistent with the EDX spectra in Fig. 4(b), where the peaks associated with corrosion-related deposits are less intense after surface treatment. Thus, the representative spectral evidence is in good agreement with the data presented in Table 5.

A further comparison of the two layer-thickness conditions indicates that the 60 µm samples generally contain higher Na and Cl contents than the 20 µm samples, both before and after shot peening. This suggests that, under the present processing and exposure conditions, the thicker-layer specimens are more susceptible to the formation or retention of corrosion products. Nevertheless, shot peening produces a clear reduction in Na and Cl content in both groups, confirming its beneficial effect irrespective of layer thickness.

Overall, the EDX results demonstrate that shot peening reduces NaCl-related corrosion products on the corroded surfaces of the additively manufactured samples. However, the observed reduction in Na and Cl content after shot peening may not exclusively reflect improved corrosion resistance. The mechanical action of shot peening can partly remove loosely adhered surface deposits, and the inherently localised and semi-quantitative nature of EDX analysis introduces the possibility of measurement variability across different surface regions.

Therefore, these findings should be interpreted as supporting evidence for reduced corrosion product accumulation, rather than as direct proof of enhanced corrosion resistance. The primary quantitative evidence for improved corrosion performance is provided by the immersion weight-loss corrosion rate data presented in Table 4, while the EDX results offer complementary microstructural support for the observed trends.

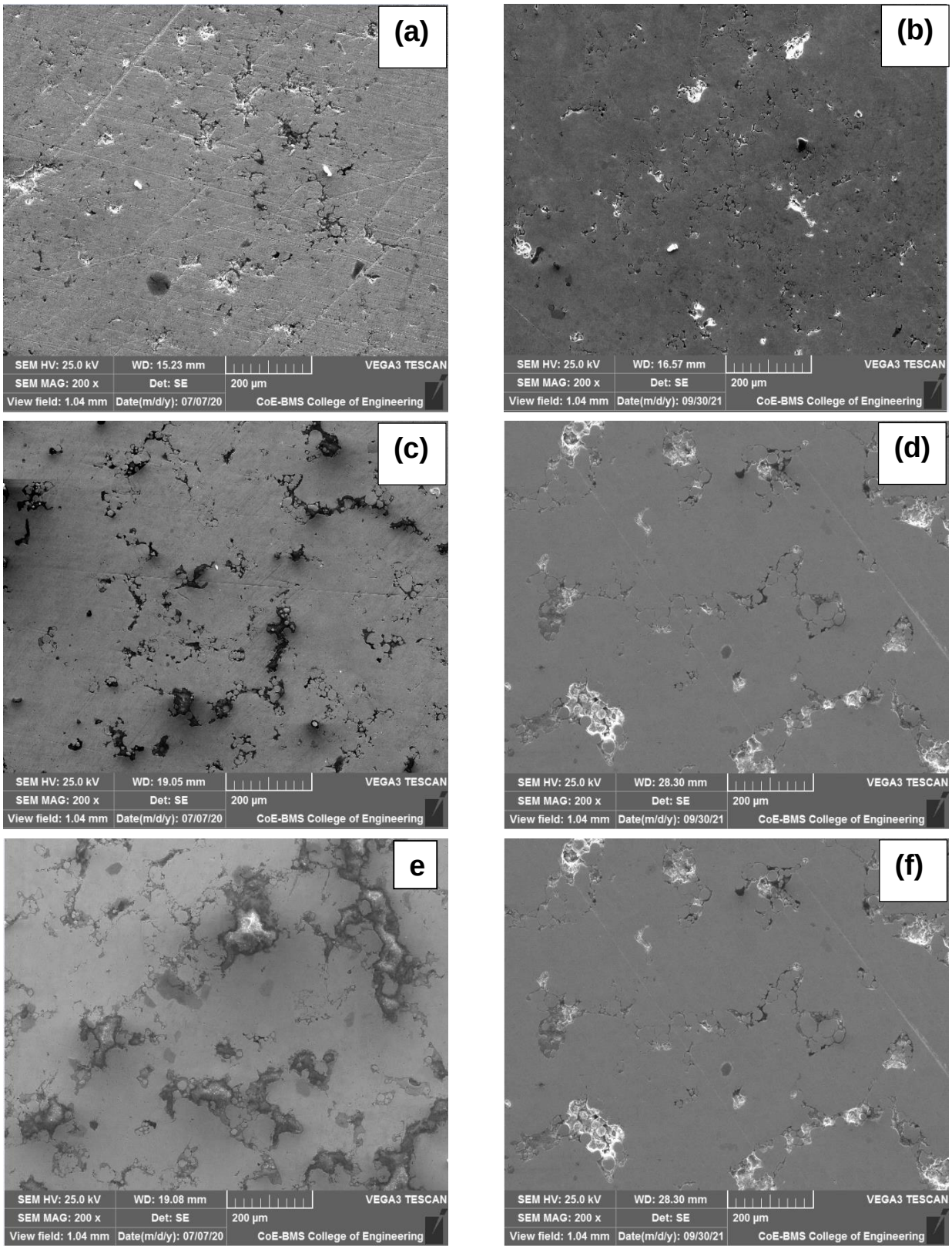

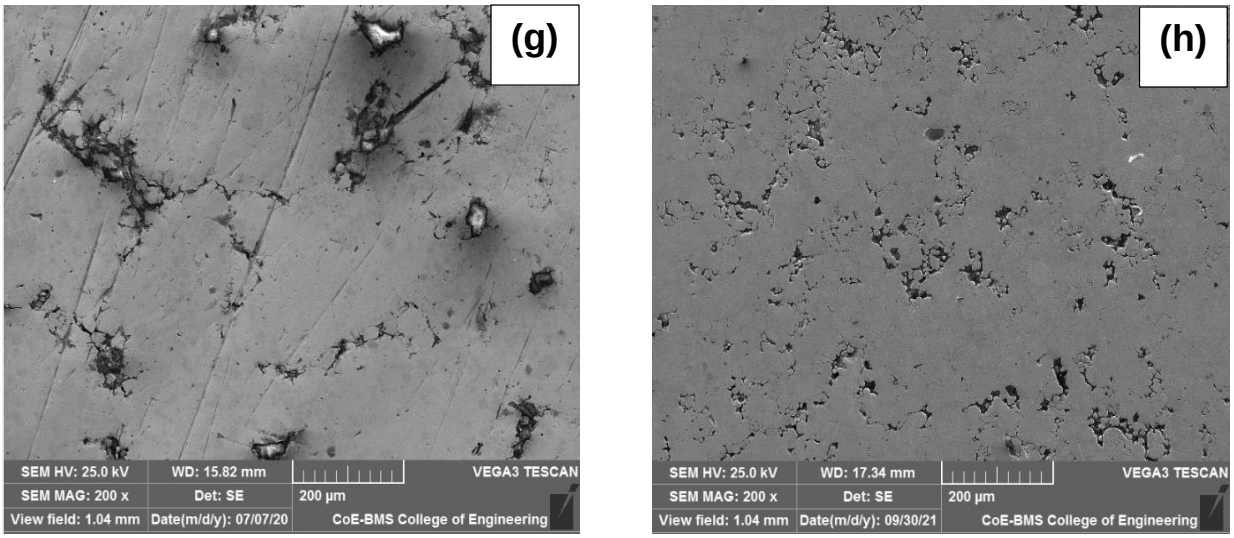

Figure (3): SEM images of corroded surfaces of DMLS-fabricated Cu–Ni alloy samples after 720 h immersion in 3% NaCl solution, showing the as-built condition (before shot peening, odd-lettered panels) alongside the shot-peened condition (after shot peening, even-lettered panels) for each sample. (a, b) Sample 120 (100 mm/s, 20 µm); (c, d) Sample 160 (100 mm/s, 60 µm); (e, f) Sample 320 (300 mm/s, 20 µm); (g, h) Sample 360 (300 mm/s, 60 µm). Within each pair, the left image (a, c, e, g) represents the as-built surface before shot peening, and the right image (b, d, f, h) represents the surface after shot peening. All images acquired at 200× magnification, 25.0 kV accelerating voltage, secondary electron (SE) detector (VEGA3 TESCAN).

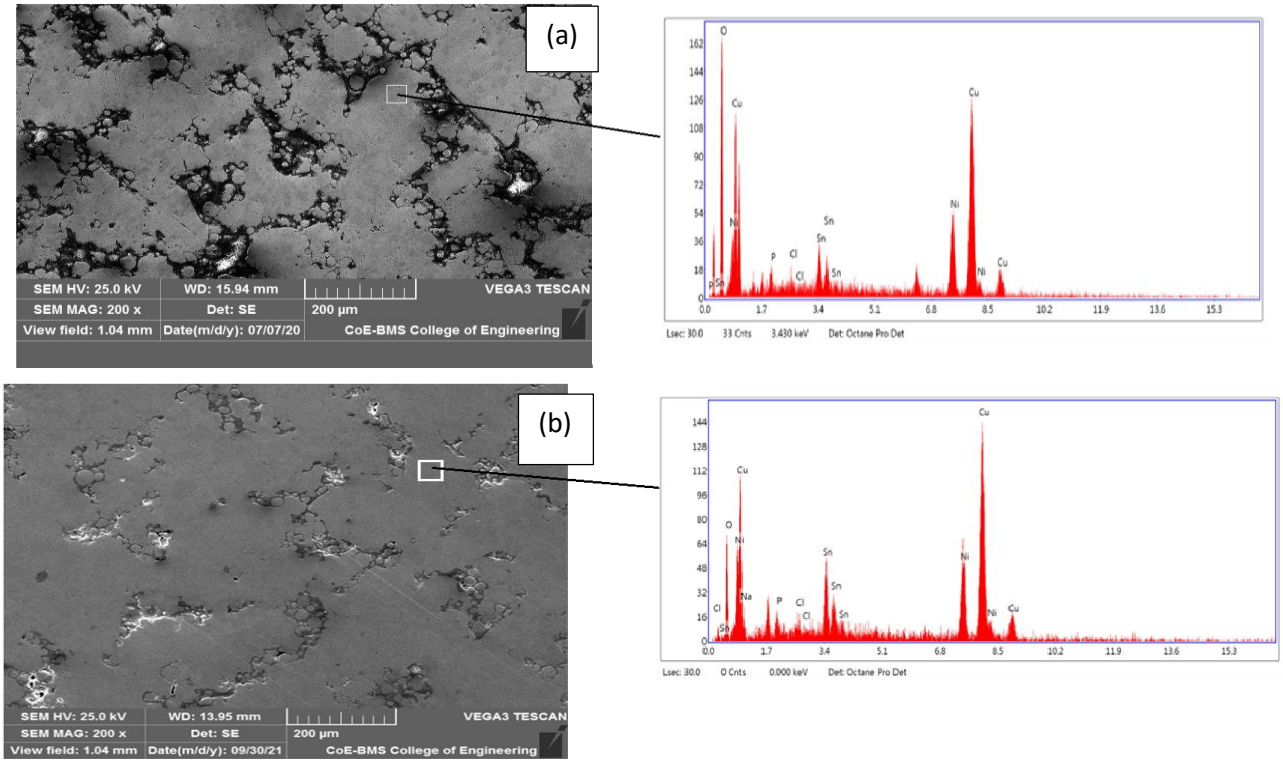

Figure (4): SEM micrographs of the corroded surface of representative sample 360 showing the region selected for EDX analysis: (a) before shot peening and (b) after shot peening.

Table (5): Chemical composition (wt.%) of corrosion products on DMLS-fabricated Cu–Ni alloy surfaces after 720 h immersion in 3% NaCl solution, before and after shot peening (SP), as determined by EDX analysis. Values represent measurements obtained from multiple representative locations on each specimen.

Alloy Designation	Laser scan speed (mm/s)	Layer thickness	Sodium (Na) Wt. %		Chlorine (Cl) Wt. %	
			Before SP	After SP	Before SP	After SP
120	100	20 µm	11.2	6.8	0.68	0.28
220	200		12.7	7.5	0.71	0.3
320	300		13.1	7.9	0.84	0.36
160	100	60 µm	13.3	8	1.14	0.46
260	200		13.9	8.2	1.67	0.62
360	300		14.3	8.7	2	0.72

Conclusion

This study presents the first systematic parametric investigation linking DMLS build conditions (laser scan speed: 100–300 mm/s; layer thickness: 20–60 µm) directly to post-shot-peening surface integrity and corrosion performance in Cu–Ni alloys. The following key conclusions are drawn from the experimental results. In the as-built condition, increasing scan speed and layer thickness degraded all measured surface integrity metrics: hardness decreased from 146 VHN to 65 VHN, surface roughness Ra increased from 6.1 µm to 12.3 µm, and corrosion rate increased from 0.67 mm/y to 1.74 mm/y,

attributable to reduced volumetric energy density leading to increased porosity and lack-of-fusion defects. Shot peening consistently improved all surface integrity metrics across all nine conditions: hardness increased by 15–30%, Ra decreased by 25–36%, compressive residual stress magnitudes increased by 40–55 MPa, and corrosion rate was reduced by 52.8–77%. The mechanistic basis - pore closure, near-surface grain refinement, and compressive residual stress induction was corroborated by SEM and EDX evidence. EDX analysis showed reductions in Na and Cl content of 37-43% and 59-64% respectively after SP, supporting reduced NaCl-related corrosion product accumulation, though it is acknowledged that mechanical surface cleaning and EDX measurement variability may also contribute to these reductions. The optimal condition 20 µm layer thickness, 100 mm/s scan speed, followed by shot peening produced a hardness of 163 VHN, Ra of 3.9 µm, a compressive residual stress of −155 MPa, and the lowest corrosion rate of 0.15 mm/y (77% reduction from as-built). These findings establish shot peening as an effective and practically viable post-processing route for DMLS-fabricated Cu–Ni components for marine and chemically aggressive applications. Future work should investigate electrochemical corrosion kinetics, fatigue performance, and long-term residual stress stability under cyclic marine loading.

Disclosure Statement

- **Ethics approval and consent to participate:** Not applicable
- **Consent for publication:** Not applicable
- **Availability of data and materials:** The raw data required to reproduce these findings are available in the body and illustrations of this manuscript.
- **Author's contribution: Rajesh R:** Conceptualization, Methodology, Investigation, Data Curation, Writing - Original Draft. **Mithun Vinayaka Kulkarni:** Conceptualization, Supervision, Validation, Writing - Review & Editing, Corresponding Author. **Bincy Rose Vergis:** Formal Analysis, Visualization, Writing – Review & Editing. **P Sampathkumaran:** Supervision, Technical Guidance, Validation, Review & Editing. **S Anand Kumar:** Supervision, Technical Guidance, Validation, Review & Editing
- All authors reviewed the results and approved the final version of the manuscript.
- **Funding:** Not Applicable
- **Conflicts of interest:** The authors declare that there is no conflict of interest regarding the publication of this article
- **Use of AI Declaration:** The authors declare that an artificial intelligence (AI)-assisted tool (Chat-GPT) was used solely to support language editing, sentence refinement, and improvement of readability during manuscript preparation. The AI tool did not generate experimental data, results, figures (except the graphical abstract), or scientific conclusions. All technical content, analysis, interpretation, and final revisions were critically evaluated and approved by the authors, who accept full responsibility for the contents of the manuscript.
- **Acknowledgements:** The authors gratefully acknowledge the Management of the Central Manufacturing Technology Institute (CMTI) for providing the facilities for the fabrication of the 3D-printed samples. The authors also wish to thank the Management of Global Academy of Technology, the University of Technology and Applied Sciences–Salalah, Sambram Institute, and BMS Institute of Technology for their support and for making available the laboratory facilities required for the experimental investigations. The authors further extend their thanks to the Management of BMS College of Engineering, Bengaluru, for providing the necessary facilities to carry out the supporting tests.

Open Access

References

1] Amer M, Lin CC, Ismail H, Wu SH, Lu BR, Wu ZY, et al. Planetary Gearbox Design and Development using Additive Manufacturing. An-Najah University Journal for Research - A. 2024 Feb;38(1):48–53. doi:10.35552/anujr.a.38.1.2150

2] Tofail SAM, Koumoulos EP, Bandyopadhyay A, Bose S, O'Donoghue L, Charitidis C. Additive manufacturing: Scientific and technological challenges, market uptake and opportunities. Materials Today. 2018;21(1):22–37. doi:10.1016/j.mattod.2017.07.001

3] DebRoy T, Wei HL, Zuback JS, Mukherjee T, Elmer JW, Milewski JO, et al. Additive manufacturing of metallic components – Process, structure and properties. Progress in Materials Science. 2018;92:112–224. doi:10.1016/j.pmatsci.2017.10.001

4] Shaqour A, Shaqour B, Shaqour A. The use of 3D Printing Technologies in Education: A Bibliometrics Review of the literature between 2004 and 2023. An-Najah University Journal for Research - A. 2026 Feb;40(1):29–36. doi:10.35552/anujr.a.40.1.2373

5] Direct Metal Laser Sintering (DMLS) - Additive Manufacturing | CustomPartNet Library [Internet]. [cited 2026 Jan 10]. Available from: https://www.custompartnet.com/library/direct-metal-laser-sintering

6] Eren O, Sezer HK, Yüksel N, Bakhtarı AR, Canyurt OE. Investigation on selective laser-melted AlSi10Mg micro-struts: influence of processing parameters on dimensional accuracy, molten pool morphology and microhardness. Rapid Prototyping Journal. 2024 Jul 30;30(8):1556–78. doi:10.1108/RPJ-05-2023-0164

7] King WE, Barth HD, Castillo VM, Gallegos GF, Gibbs JW, Hahn DE, et al. Observation of keyhole-mode laser melting in laser powder-bed fusion. Journal of Materials Processing Technology. 2014;214(12):2915–25. doi:10.1016/j.jmatprotec.2014.06.005

8] Mugwagwa L, Yadroitsev I, Matope S. Effect of process parameters on residual stresses, distortions, and porosity in selective laser melting. Metals. 2019;9(10):1042. doi:10.3390/met9101042

9] Rajesh R, Kulkarni MV, Vergis BR, Sampathkumar P, Seetharamu S. Copper–nickel alloys made using direct metal laser sintering method for assessing corrosion

resistance properties. Materials Today: Proceedings. 2021;45:5555–61. doi:10.1016/j.matpr.2021.05.178

10] Xie X, Zhang L, Zhu L, Li Y, Hong T, Yang W, et al. State of the Art and Perspectives on Surface-Strengthening Process and Associated Mechanisms by Shot Peening. Coatings. 2023 Apr 30;13(5):859. doi:10.3390/coatings13050859

11] P.T. Iswanto, H. Akhyar, A. Faqihudin. Effect of shot peening on microstructure, hardness, and corrosion resistance of AISI 316L [Internet]. Vol. 89. 2018 Jan 7;89(1):19–26. doi:10.5604/01.3001.0012.6668

12] 12. Hönnige JR, Davis AE, Ho A, Kennedy JR, Neto L, Prangnell P, et al. The Effectiveness of Grain Refinement by Machine Hammer Peening in High Deposition Rate Wire-Arc AM Ti-6Al-4V. Metall Mater Trans A. 2020 Jul;51(7):3692–703. doi:10.1007/s11661-020-05781-6

13] Song Y, Wang W, Chen M, Guo J, Lingfeng Xu, Gao D, et al. Ultrafine-Grained Materials Fabrication with High Pressure Torsion and Simulation of Plastic Deformation Inhomogeneous Characteristics. In: Cabibbo M, editor. Severe Plastic Deformation Techniques [Internet]. London: IntechOpen; 2017. Available from: https://doi.org/10.5772/intechopen.68360 doi:10.5772/intechopen.68360

14] Snir Y, Ben-Hamu G, Eliezer D, Abramov E. Effect of compression deformation on the microstructure and corrosion behavior of magnesium alloys. Journal of Alloys and Compounds. 2012 Jul 5;528:84–90. doi:10.1016/j.jallcom.2012.03.010

15] AlMangour B, Yang JM. Improving the surface quality and mechanical properties by shot-peening of 17-4 stainless steel fabricated by additive manufacturing. Materials & Design. 2016 Nov 15;110:914–24. doi:10.1016/j.matdes.2016.08.037

16] Calignano F, Manfredi D, Ambrosio EP, Iuliano L, Fino P. Influence of process parameters on surface roughness of aluminum parts produced by DMLS. Int J Adv Manuf Technol. 2013 Aug 1;67(9):2743–51. doi:10.1007/s00170-012-4688-9

17] Maamoun AH, Elbestawi MA, Veldhuis SC, Maamoun AH, Elbestawi MA, Veldhuis SC. Influence of Shot Peening on AlSi10Mg Parts Fabricated by Additive Manufacturing. Journal of Manufacturing and Materials Processing. 2018 Jun 24;2(3). doi:10.3390/jmmp2030040

18] Gholami M. Corrosion performance of shot-peened high-strength CuNi3SiMg alloy in sodium chloride solution. Corrosion Science. 2014;78:129–38. doi:10.1016/j.corsci.2013.09.017

19] Lv Y, Zhang Z, Hu Z, Liu J. Improving corrosion resistance of nickel–aluminium bronze alloys via shot peening. Materials Transactions. 2019;60(8):1629–37. doi:10.2320/matertrans.M2019013

20] Żebrowski R, Walczak M, Klepka T, Pasierbiewicz K. Effect of the shot peening on surface properties of Ti-6Al-4V alloy produced by means of DMLS technology. Eksploatacja i Niezawodność – Maintenance and Reliability. 2019 Mar 31;21(1):46–53. doi:10.17531/ein.2019.1.6

21] Mythreyi OV, Raja A, Nagesha BK, Jayaganthan R, Mythreyi OV, Raja A, et al. Corrosion Study of Selective Laser Melted IN718 Alloy upon Post Heat Treatment and Shot Peening. Metals. 2020 Nov 24;10(12). doi:10.3390/met10121562

22] Applications of copper-nickel alloys [Internet]. [cited 2026 Apr 11]. Available from: https://nickelinstitute.org/en/nickel-applications/copper-nickel-alloys/applications-of-copper-nickel-alloys

23] Multiview. Benefits of Adding Phosphor to Copper Alloys. Belmont Metals [Internet]. 2021 Mar 10 [cited 2026 Apr 11]. Available from: https://www.belmontmetals.com/benefits-of-adding-phosphor-to-copper-alloys/

24] Effects of Copper Alloy Chemical Compositions on Corrosion [Internet]. [cited 2026 Apr 11]. Available from: https://tubingchina.com/Effects-of-Alloy-Chemical-Compositions-on-Corrosion.htm

25] Guo L, Zuo P, Zhang Z, Zhang Q, Zhao M, Hou X, et al. A Review of Cu–Ni–Sn Alloys: Processing, Microstructure, Properties, and Developing Trends. Materials (Basel). 2023 Jan 3;16(1):444. doi:10.3390/ma16010444 PubMed PMID: 36614783; PubMed Central PMCID: PMC9822053.

26] Standard Test Method for Density of Powder Metallurgy (PM) Materials Containing Less Than Two Percent Porosity [Internet]. [cited 2026 Mar 7]. Available from: https://store.astm.org/b0311-22.html

27] Raffeis I, Adjei-Kyeremeh F, Vroomen U, Westhoff E, Bremen S, Hohoi A, et al. Qualification of a Ni–Cu Alloy for the Laser Powder Bed Fusion Process (LPBF): Its Microstructure and Mechanical Properties. Applied Sciences. 2020 May 14;10(10):3401. doi:10.3390/app10103401

28] Maleki E, Bagherifard S, Bandini M, Guagliano M. Surface post-treatments for metal additive manufacturing: Progress, challenges, and opportunities. Additive Manufacturing. 2021 Jan 1;37:101619. doi:10.1016/j.addma.2020.101619

29] Pourrahimi S, Hof LA. On the Post-Processing of Complex Additive Manufactured Metallic Parts: A Review. Adv Eng Mater. 2024 May;26(10):2301511. doi:10.1002/adem.202301511

30] Yadroitsev I, Smurov I. Surface Morphology in Selective Laser Melting of Metal Powders. Physics Procedia. 2011 Jan 1;Lasers in Manufacturing 2011 - Proceedings of the Sixth International WLT Conference on Lasers in Manufacturing12:264–70. doi:10.1016/j.phpro.2011.03.034

31] Strano G, Hao L, Everson RM, Evans KE. Surface roughness analysis, modelling and prediction in selective laser melting. Journal of Materials Processing Technology. 2013 Apr 1;213(4):589–97. doi:10.1016/j.jmatprotec.2012.11.011

32] Paggetti S, Bedogni E, Veronesi P. Factors Affecting the Surface Roughness of the As-Built Additively Manufactured Metal Parts: A Review. Metals. 2025 Sep 24;15(10):1069. doi:10.3390/met15101069

33] Prevey PS. X-Ray Diffraction Residual Stress Techniques. In: Metals Handbook. Metals Park, OH: American Society for Metals; 1986. p. 380–92.

34] Withers PJ, Bhadeshia HKDH. Residual stress. Part 1 – Measurement techniques. Materials Science and Technology. 2001 Apr 1;17(4):355–65. doi:10.1179/026708301101509980

35] Noyan IC, Cohen JB. Fundamental Concepts in Stress Analysis. In: Noyan IC, Cohen JB, editors. Residual Stress: Measurement by Diffraction and Interpretation [Internet]. New York, NY: Springer; 1987 [cited 2026 Mar 31]. p. 13–46. Available from: https://doi.org/10.1007/978-1-4613-9570-6_2 doi:10.1007/978-1-4613-9570-6_2

36] Noyan IC, Cohen JB. Fundamental Concepts in X-ray Diffraction. In: Noyan IC, Cohen JB, editors. Residual Stress:

Measurement by Diffraction and Interpretation [Internet]. New York, NY: Springer; 1987 [cited 2026 Mar 31]. p. 75–116. Available from: https://doi.org/10.1007/978-1-4613-9570-6_4 doi:10.1007/978-1-4613-9570-6_4

37] Fitzpatrick ME, Fry AT, Holdway P, Kandil FA, Shackleton J, Suominen L. Determination of Residual Stresses by X-ray Diffraction, Measurement Good Practice Guide No. 52. UK, London: National Physical Laboratory; 2005. 77 p.

38] Noyan IC, Cohen JB. Residual Stress [Internet]. New York, NY: Springer; 1987 [cited 2026 Mar 31]. Available from: http://link.springer.com/10.1007/978-1-4613-9570-6 doi:10.1007/978-1-4613-9570-6

39] Shen X, Shukla P, Subramaniyan AK, Zammit A, Swanson P, Lawrence J, et al. Residual stresses induced by laser shock peening in orthopaedic Ti-6Al-7Nb alloy. Optics & Laser Technology. 2020 Nov 1;131:106446. doi:10.1016/j.optlastec.2020.106446

40] Chen H, Guan Y, Zhu L, Li Y, Zhai J, Lin J. Effects of ultrasonic shot peening process parameters on nanocrystalline and mechanical properties of pure copper surface. Materials Chemistry and Physics. 2021 Feb 1;259:124025. doi:10.1016/j.matchemphys.2020.124025

41] Gajera HM, Dave KG, Darji VP, Abhishek K. Optimization of process parameters of direct metal laser sintering process using fuzzy-based desirability function approach. J Braz Soc Mech Sci Eng. 2019 Feb 13;41(3):124. doi:10.1007/s40430-019-1621-2

42] Deng C, Kang J, Feng T, Feng Y, Wang X, Wu P, et al. Study on the Selective Laser Melting of CuSn10 Powder. Materials. 2018 Apr 17;11(4). doi:10.3390/ma11040614

43] Damon J, Dietrich S, Vollert F, Gibmeier J, Schulze V. Process dependent porosity and the influence of shot peening on porosity morphology regarding selective laser melted AlSi10Mg parts. Additive Manufacturing. 2018 Mar 1;20:77–89. doi:10.1016/j.addma.2018.01.001

44] Aguado-Montero S, Navarro C, Vázquez J, Domínguez J. Fatigue behaviour of powder bed fusion Ti-6Al-4V after shot and laser peening. International Journal of Fatigue. 2022;154:106556. doi:10.1016/j.ijfatigue.2021.106556

45] Vahedi Nemani A, Ghaffari M, Sabet Bokati K, Valizade N, Afshari E, Nasiri A. Advancements in Additive Manufacturing for Copper-Based Alloys and Composites: A Comprehensive Review. JMMP. 2024 Mar 2;8(2):54. doi:10.3390/jmmp8020054

46] Ali H, Ghadbeigi H, Mumtaz K. Processing Parameter Effects on Residual Stress and Mechanical Properties of Selective Laser Melted Ti6Al4V. J of Materi Eng and Perform. 2018 Aug 1;27(8):4059–68. doi:10.1007/s11665-018-3477-5

47] Liu Y, Yang Y, Mai S, Wang D, Song C. Influence of laser scanning speed on densification of selective laser melted AlSi10Mg alloy. Journal of Materials Processing Technology. 2015;220:12–9. doi:10.1016/j.jmatprotec.2015.01.004

48] Bagherifard S, Guagliano M. Nanoscale surface modification of AISI 316L stainless steel by severe shot peening. Materials & Design. 2016;102:68–77. doi:10.1016/j.matdes.2016.04.012

49] Rajesh R, Kulkarni M, Sampathkumaran P, Kumar S, Seetharamu S, Katiyar J. Tribological Performance Involving DOE of an Additively Manufactured Cu-Ni Alloy. In. 2022. p. 75–96. doi:10.1201/9781003243205-5

50] Shang Y, Yuan Y, Li D, Li Y, Chen J. Effects of scanning speed on in vitro biocompatibility of 316L stainless steel parts elaborated by selective laser melting. Int J Adv Manuf Technol. 2017 Oct 1;92(9):4379–85. doi:10.1007/s00170-017-0525-5

51] Liu Y, Shi J, Wang Y. Evolution, Control, and Mitigation of Residual Stresses in Additively Manufactured Metallic Materials: A Review. Advanced Engineering Materials. 2023;25(22):2300489. doi:10.1002/adem.202300489

52] Okuniewski W, Fliegener S, Schubnell J, Wegener K. Effects of shot peening and electropolishing on additively and conventionally manufactured Ti-6Al-4V: A review. Materials. 2024;17(4):934. doi:10.3390/ma17040934